September 16, 2013

Aerodynamic Simulation of Vertical-Axis Wind Turbines

A. Korobenko, *University of California, San Diego*
Ming-Chen Hsu, *University of Texas-Austin*
I. Akkerman, *Durham University*
Y. Bazilevs, *University of California, San Diego*

A. Korobenko
Department of Structural Engineering,
University of California-San Diego,
La Jolla, CA 92093

M.-C. Hsu
Institute for Computational
Engineering and Sciences,
University of Texas-Austin,
Austin, TX 78712

I. Akkerman
School of Engineering and Computing Sciences,
Durham University,
Durham, UK

Y. Bazilevs
Department of Structural Engineering,
University of California-San Diego,
La Jolla, CA 92093
e-mail: yuri@ucsd.edu

Aerodynamic Simulation of Vertical-Axis Wind Turbines

Full-scale, 3D, time-dependent aerodynamics modeling and simulation of a Darrieus-type vertical-axis wind turbine (VAWT) is presented. The simulations are performed using a moving-domain finite-element-based ALE-VMS technique augmented with a sliding-interface formulation to handle the rotor-stator interactions present. We simulate a single VAWT using a sequence of meshes with increased resolution to assess the computational requirements for this class of problems. The computational results are in good agreement with experimental data. We also perform a computation of two side-by-side counterrotating VAWTs to illustrate how the ALE-VMS technique may be used for the simulation of multiple turbines placed in arrays. [DOI: 10.1115/1.4024415]

1 Introduction

During the last several decades engineers and scientists put significant effort into developing reliable and efficient wind turbines. Since the 1970s most of the work focused on the development of horizontal-axis wind turbines (HAWTs). Vertical-axis wind turbines (VAWTs) were generally considered as a promising alternative to HAWTs. Before the mid-1990s VAWTs were economically competitive with HAWTs for the same rated power. However, as the market demands for electric power grew, VAWTs were found to be less efficient than HAWTs for large-scale power production. As wind energy technologies matured, VAWTs recently resurfaced as a good source of small-scale electric power for urban areas. The main reason for this is their compact design. The gearbox and drive train components are located on the ground, which allows easier access, installation, maintenance, and repair. Another advantage is VAWTs can respond to the wind coming from any direction, which obviates the need to include expensive yaw control mechanisms in their design. The disadvantages of VAWTs include their relatively low efficiency compared to HAWTs and issues related to self-starting. The ability to self-start depends on the wind conditions and necessitates the use of an additional starting system as part of the VAWT design.

There are two main configurations of VAWTs: The Savonius and Darrieus rotor types [1]. The former is a drag-type turbine, where the power is generated using momentum transfer. In contrast to the Savonius configuration, the Darrieus configuration is a lift-driven turbine: The power is produced from the aerodynamic torque acting on the rotor. The efficiency of Darrieus-type turbines is significantly higher than that of the Savonius-type, and it is for this reason we focus on Darrieus-type turbines in this work.

Aerodynamic simulation of VAWTs, in our opinion, is more challenging than that of HAWTs for the following reasons. In the case of VAWTs, even under steady wind and rotor speeds, the flow angle-of-attack is constantly changing. For most cases of interest these changes are significant, and the flow constantly transitions from fully attached to separated. As a result, even under steady operating conditions, this creates truly unsteady turbulent aerodynamics. High-fidelity modeling of the underlying aerodynamics requires a numerical formulation that properly accounts for this flow unsteadiness and is valid for all flow regimes present. It is precisely this unsteady nature of the flow that creates significant challenges for the application of low-fidelity methods and tools (such as, for example, the FAST code [2]) to VAWTs. Another challenge is to represent how the turbulent flow features generated by the upstream blades affect the aerodynamics of the downstream blades [3]. The VAWT simulation complexity is further increased when several VAWTs are operating in close proximity to one another. Due to their compact design, VAWTs are often placed in arrays with spacing that is a little over one diameter between the turbine towers. In Ref. [4], this type of placement was found beneficial for increased energy production.

The above challenges are addressed in this work. The aerodynamics of VAWTs is simulated using a finite-element-based ALE-VMS technique. ALE-VMS [5,6] was successfully employed for the aerodynamics simulation of HAWTs in Refs. [7–10], and fluid–structure interaction (FSI) simulation of HAWTs in Refs. [11–14]. The sliding interface formulation employed in conjunction with the ALE-VMS technique enables the simulation of the interaction between the spinning rotor and stationary tower, as well as the simulation of multiple wind turbines and interaction between them. The sliding interface formulation was developed in Ref. [15] and used in the computation of HAWTs in Ref. [9], including FSI coupling in Ref. [13]. In addition, for improved boundary-layer accuracy, a key ingredient employed in the ALE-VMS simulation of wind-turbine aerodynamics and FSI is the weakly enforced no-slip boundary conditions [16–18] set on the moving blade surfaces.

In this article, the techniques we previously developed for HAWTs are directly applied to the simulation of VAWTs. The main goals of this paper are to illustrate the capability and assess the accuracy and computational costs of the techniques for this new challenging class of problems. We note that recently a few articles were published on 2D and 3D modeling and simulation of VAWTs [19–22]. However, rather than solving the time-dependent problem, a quasi-static representation of the air flow was employed in Ref. [22]. Furthermore, only a single VAWT was simulated in the articles cited.

The paper is outlined as follows. In Sec. 2 we present the governing equations of aerodynamics, including compatibility conditions at the sliding interface between the moving and stationary domains. In Sec. 3 we show the computations of a small-scale Darrieus-type wind turbine. For the simulations presented the

Contributed by Applied Mechanics of ASME for publication in the JOURNAL OF APPLIED MECHANICS. Manuscript received February 17, 2013; final manuscript received April 7, 2013; accepted manuscript posted May 7, 2013; published online September 16, 2013. Assoc. Editor: Kenji Takizawa.

wind turbine geometry and wind tunnel test data were taken from Refs. [22,23]. We simulate two cases: a single turbine, and two counterrotating turbines placed side-by-side in close proximity to one another. For a single turbine we perform a mesh refinement study, and compare the results to experimental data. In Sec. 4 we draw conclusions and highlight future research directions.

2 Methods for Modeling and Simulation of VAWT Aerodynamics

The VAWT aerodynamics is governed by the Navier–Stokes equations of incompressible flows. The incompressible-flow assumption is valid for our application due to low values of the Mach number in these flows. The Navier–Stokes equations in the arbitrary Lagrangian–Eulerian (ALE) frame [24] can be written as follows:

$$\rho\left(\left.\frac{\partial \mathbf{u}}{\partial t}\right|_{\hat{x}} + (\mathbf{u}-\hat{\mathbf{u}})\cdot\nabla\mathbf{u} - \mathbf{f}\right) - \nabla\cdot\boldsymbol{\sigma} = \mathbf{0} \tag{1}$$

$$\nabla\cdot\mathbf{u} = 0 \tag{2}$$

where ρ is the density, $\mathbf{f}$ is the external force per unit mass, $\mathbf{u}$ and $\hat{\mathbf{u}}$ are velocities of the fluid and fluid domain, respectively. The stress tensor $\boldsymbol{\sigma}$ is defined as

$$\boldsymbol{\sigma}(\mathbf{u},p) = -p\mathbf{I} + 2\mu\boldsymbol{\varepsilon}(\mathbf{u}) \tag{3}$$

where p is the pressure, $\mathbf{I}$ is the identity tensor, μ is the dynamic viscosity, and $\boldsymbol{\varepsilon}(\mathbf{u})$ is the strain-rate tensor given by

$$\boldsymbol{\varepsilon}(\mathbf{u}) = \frac{1}{2}\left(\nabla\mathbf{u} + \nabla\mathbf{u}^T\right) \tag{4}$$

In Eq. (1), $|_{\hat{x}}$ denotes the time derivative taken with respect to a fixed referential domain spatial coordinates $\hat{\mathbf{x}}$. The spatial derivatives in the above equations are taken with respect to the spatial coordinates $\mathbf{x}$ of the current configuration.

To model a single VAWT, we decompose the problem domain into two subdomains: a rotating cylindrical domain that encloses the rotor and a stationary domain that contains a portion of the tower below the rotor and all the inlet, outlet, and lateral boundaries. As the rotor spins, the cylindrical domain rotates with it, which creates a sliding interface between the two subdomains. The compatibility conditions enforced at the sliding interface are

$$\mathbf{u}_M - \mathbf{u}_S = 0 \tag{5}$$

$$(-p_S\mathbf{I} + 2\mu\boldsymbol{\varepsilon}(\mathbf{u}_S))\mathbf{n}_S + (-p_M\mathbf{I} + 2\mu\boldsymbol{\varepsilon}(\mathbf{u}_M))\mathbf{n}_M = 0 \tag{6}$$

where all quantities with subscripts "S" and "M" refer to the stationary and moving subdomains, respectively (see Fig. 1), and $\mathbf{n}_S$ and $\mathbf{n}_M$ are the unit outward normal vectors. In the case of multiple VAWTs, each rotor is enclosed by its spinning cylindrical subdomain, and multiple sliding interfaces are present in the computation where the compatibility conditions given by Eqs. (5) and (6) are enforced. The discrete formulation is obtained using the ALE-VMS method with weakly enforced boundary conditions and the appropriate numerical treatment of the sliding interface (see Ref. [25] for the details of the methods). Low-order FEM is used for spatial discretization, and the generalized-α method [26–28] is employed to advance the ALE-VMS equations in time.

Remark. We note that rotation is handled with the ALE technique rather than using the Navier–Stokes equations written in the rotating reference frame. We favor using ALE (or other moving-domain techniques, such as space–time methods [29–37]) for this class of problems because it naturally leads to a kinematically consistent treatment of rotor-stator interaction.

Remark. We note that in application of the FEM to flows with moving mechanical components, the shear–slip mesh update method [38–40] and its more general versions [41,42] may also be used to handle objects in relative motion.

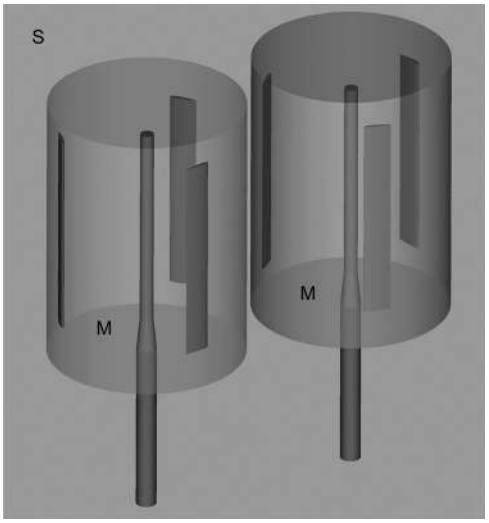

Fig. 1 Computational domain for the two-VAWT case: zoom on the rotating subdomains. The two cylindrical subdomains (labeled "M") spin with the rotors, while the remaining subdomain (labeled "S") is stationary.

3 Computational Results

The aerodynamics simulations are performed for a three-blade, high-solidity VAWT with the rated power of 3.5 kW. The prototype is a Darrieus H-type turbine designed by Cleanfield Energy Corporation. Full-scale tests for this turbine were conducted in the National Research Council (NRC) low-speed wind tunnel at McMaster University. Experimental studies for this turbine focused on the application of VAWTs in urban areas [23].

The turbine has a tower height of 7 m. The blades, 3 m in height, are connected to the tower by the struts of length 1.25 m. This value is taken as the rotor radius. A symmetric NACA0015 airfoil profile with chord length of 0.4 m is employed along the entire length of the blades. See Fig. 1 for an illustration.

The computations were carried out for constant inflow wind speed of 10 m/s and constant rotor speed of 115 rpm. This setup corresponds to the tip speed ratio of 1.5, which gave maximum rotor power as reported in Refs. [22,23]. However, it was also reported for the wind tunnel tests that the control mechanism employed was able to maintain an *average* rotor speed of 115 rpm with the deviation of ± 2.5 rpm. This means the actual rotor speed was never constant.

The air density and viscosity are set to 1.23 kg/m^3 and 1.78×10^{-5} kg/(m·s), respectively. On the inflow, the wind speed of 10 m/s is prescribed. On the top, bottom, and side surfaces of the stationary domain no-penetration boundary conditions are prescribed, while a zero traction boundary condition is set on the outflow. No-slip boundary conditions are imposed weakly on the rotor blades and tower. The struts are not modeled in this work to reduce computational cost. The struts are not expected to significantly influence the results for this VAWT design.

The computations were carried out in a parallel computing environment. The meshes, which consist of linear triangular prisms in the boundary layers and linear tetrahedra elsewhere, are partitioned into subdomains using METIS software [43], and each subdomain is assigned to a compute core. The parallel implementation of the methodology may be found in Ref. [8]. The time step is set to 1.0×10^{-5} s for all cases.

3.1 Single Turbine Simulation. We first compute a single VAWT and assess the resolution demands for this class of

Table 1 Statistics of the FEM meshes of the VAWT

	Number of nodes	Number of elements
Mesh 1	1,143,609	4,064,358
Mesh 2	2,478,993	7,324,964
Mesh 3	6,401,238	17,434,372

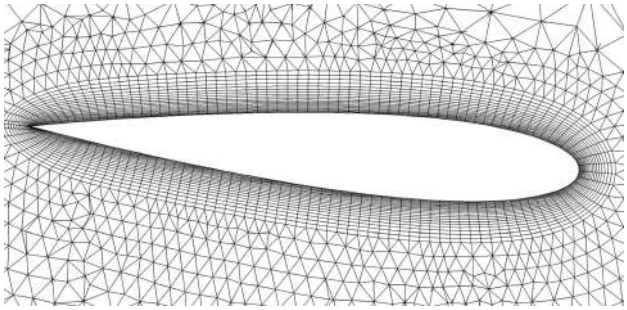

Fig. 2 Blade cross-section boundary layer of mesh 2

problems. The stationary domain has the outer dimensions of 50 m, 20 m, and 30 m in the streamwise, vertical, and spanwise directions, respectively. The VAWT centerline is located 15 m from the inflow and side boundaries. The radius and height of the spinning cylinder are both 4 m.

Three meshes are used with increasing levels of refinement. The overall mesh statistics are summarized in Table 1. The finest mesh has over 17 million elements. The details of the boundary-layer discretization are as follows. For mesh 1, the size of the first element in the wall-normal direction is 0.667 mm, and 15 layers of prismatic elements were generated with a growth ratio of 1.15. For mesh 2, the size of the first element in the wall-normal direction is 0.470 mm, and 21 layers of prismatic elements were generated with a growth ratio of 1.1. For mesh 3, the size of the first element in the wall-normal direction is 0.333 mm, and 30 layers of prismatic elements were generated with a growth ratio of 1.05. Figure 2 shows a 2D slice of mesh 2, focusing on the boundary-layer discretization of the blade.

Time history of the computed aerodynamic torque is plotted in Fig. 3 together with the experimental value reported for these operating conditions. Only the mean value of the torque was

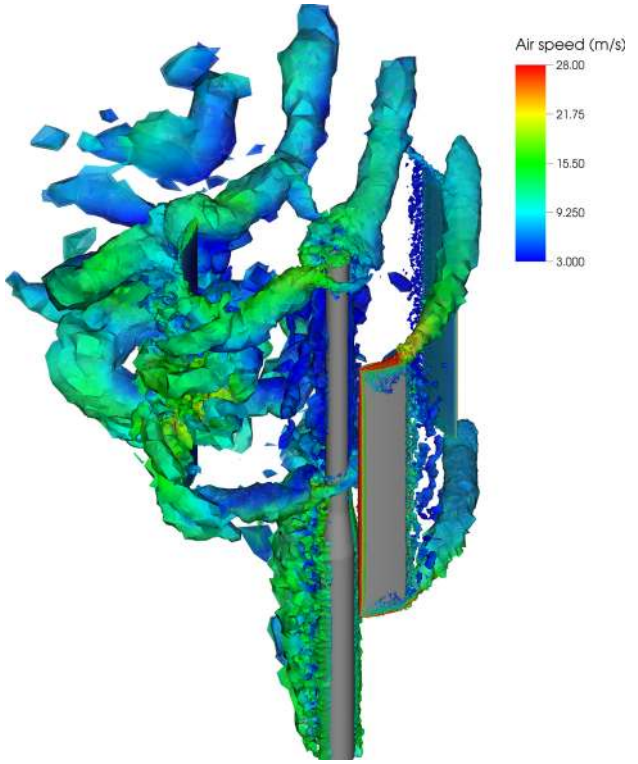

Fig. 4 Vorticity isosurfaces at a time instant colored by velocity magnitude

reported in Refs. [22,23]. Note that after a couple of cycles a nearly periodic solution is attained. Mesh 1 predicts the average torque of about 52 Nm, mesh 2 gives the average torque of about 70 Nm, and mesh 3 predicts the average torque of about 80 Nm, while the targeted experimental value is about 90 Nm. Looking further at the curves we observe that the largest differences between the predicted values of the torque between the meshes occur at the maxima and minima of the curves. Also note that the torque fluctuation during the cycle is nearly 200 Nm, which is over twice the average. One way to mitigate such high torque variations is to allow variable rotor speed.

Figure 4 shows a snapshot of vorticity colored by flow speed. The upstream blade generates tip vortices near its top and bottom

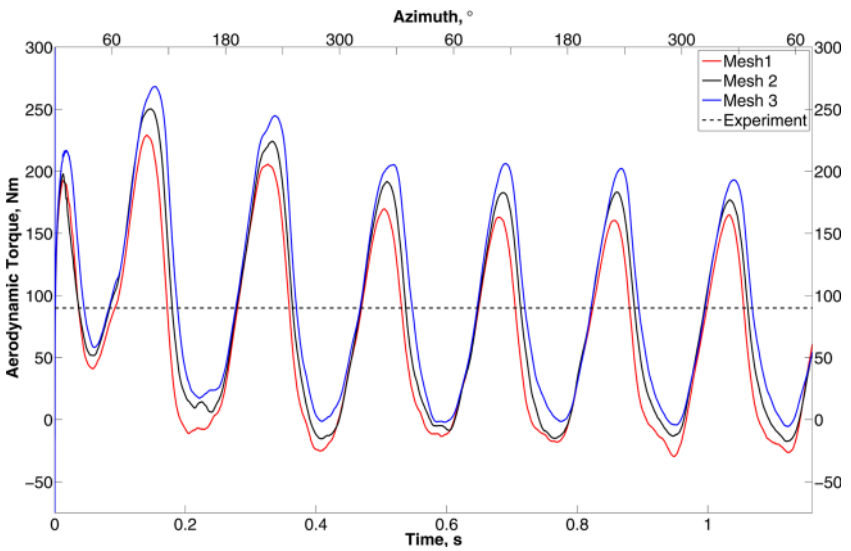

Fig. 3 Time history of the aerodynamic torque for the three meshes used. The experimental result is plotted for comparison.

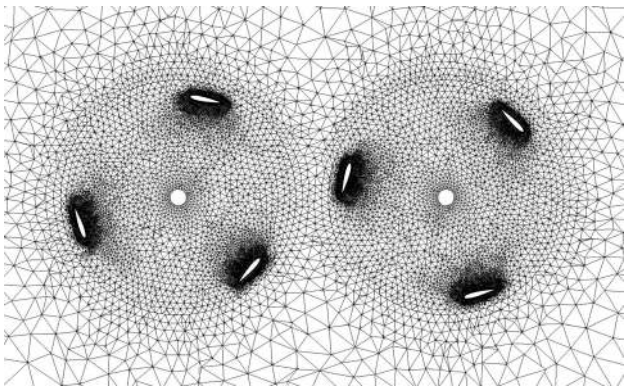

Fig. 5 Cross section of the mesh for the two-VAWT case

sections. Note that no large vortices are present in the middle section of the blade. There, as the flow separates on the airfoil surface, larger vortices immediately break up into fine-grained trailing-edge turbulence. The tip vortex and trailing-edge turbulence are then convected with the ambient wind velocity, and impact the tower, as well as the blade that happens to be in the downwind position in the spin cycle. However, as it is evident from the torque time histories shown in Fig. 3, these do not produce a major impact on the rotor loads, at least for a chosen set of wind and rotor speeds. The situation may, of course, change for a different set of operating conditions.

3.2 Multiple Turbine Simulation. Here we investigate two counterrotating turbines placed side-by-side in close proximity to one another. The wind and rotor speeds are the same as before, however, the turbines rotate out of phase, with the difference of 60 deg. The distance between the towers of the two turbines is $2.64R$, where $R = 1.25$ m is the rotor radius. This distance between the turbines falls in the range investigated in the experimental work of Ref. [4].

The stationary domain has the outer dimensions of 50 m, 20 m, and 33.3 m in the streamwise, vertical, and spanwise directions, respectively. The centerline of each VAWT is located 15 m from the inflow and 15 m from its closest side boundary. The radius and height of the spinning cylinders are 1.45 m and 4 m, respectively.

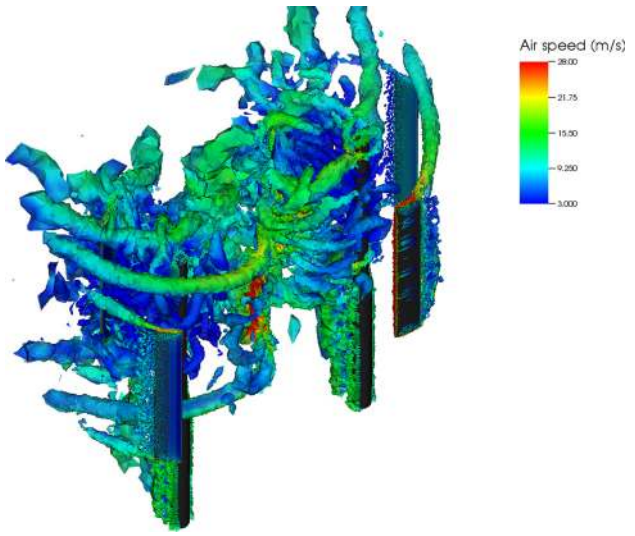

Fig. 7 Vorticity isosurfaces at a time instant colored by flow speed for two VAWTs

A 2D slice of the computational-domain mesh focusing on the two rotors is shown in Fig. 5. The boundary layer discretization employed for this computation is the same as that of mesh 2 in the Sec. 3.1.

Figure 6 shows the time history of the aerodynamic torque for the two-turbine case. The curve corresponding to the second turbine is shifted by 60 deg such that both curves are in phase. The time history of the torque for a single VAWT simulation is shown for comparison. Note that while the maxima of all curves are virtually coincident, the minima are lower for the case of multiple turbines. Also note that the multiple-turbine torque curves exhibit some fluctuation near their minima, while the single-turbine torque curve is smooth near its minima. This is likely due to the fact that the blade from one turbine, as it approaches the plane defined by the centerlines of the two towers, encounters the wake of the blade from another turbine. This, in turn, produces higher drag on that blade and results in reduction of the aerodynamic torque. A snapshot of vorticity colored by flow speed depicted in Fig. 7 shows that the short distance between the turbines has a noticeable effect on the resulting aerodynamics. This effect may be seen

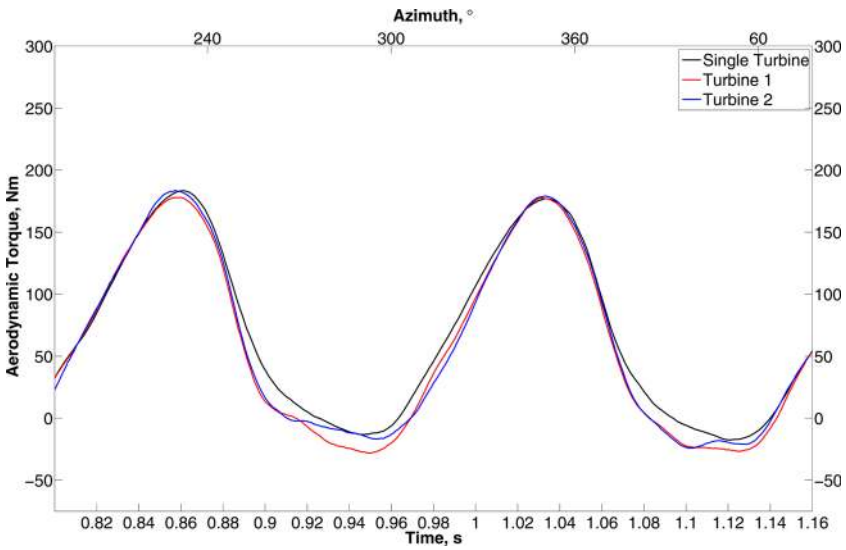

Fig. 6 Time history of the aerodynamic torque for two VAWTs. The data for the second turbine are shifted by 60 deg to be in phase with the first turbine. Results from a single turbine simulation are plotted for comparison.

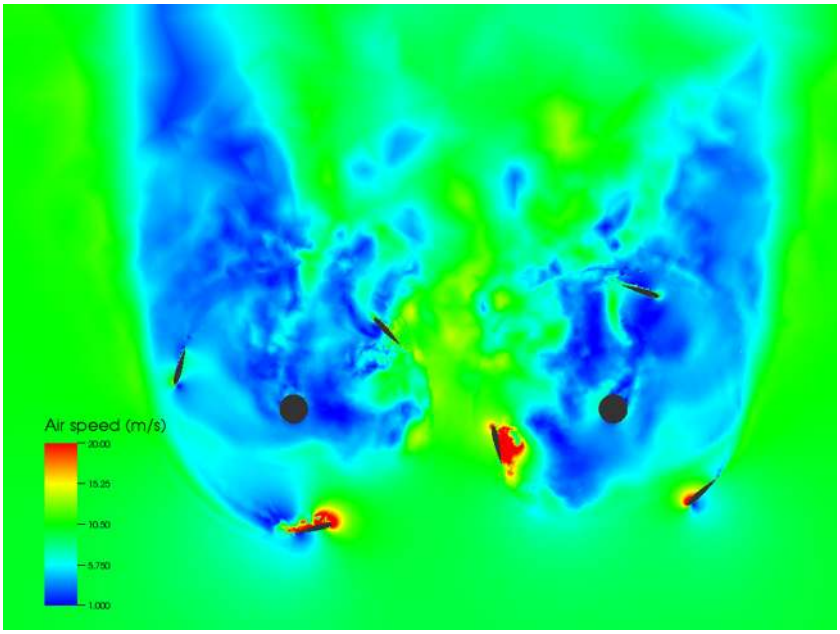

Fig. 8 Air speed at a 2D cross section for the two-VAWT case

more clearly in Fig. 8, which shows that one of the blades from the VAWT on the right is about to enter the turbulent region between the turbines.

4 Conclusions and Future Work

In this study we applied the previously developed ALE-VMS technique, in conjunction with weakly enforced boundary conditions and the sliding-interface formulation, to simulate VAWTs at full scale. A Darrieus H-type turbine was chosen as a prototype due to its relatively simple geometry as well as availability of wind tunnel test data. The inherently unsteady and turbulent nature of the flow necessitates the use of finer grids for good prediction of the aerodynamic rotor loads. A simulation of two side-by-side wind turbines was also performed. We found that the counter-rotating, out-of-phase configuration produces a slight drop in the predicted aerodynamic torque.

In the future we plan to first approximate the rotor as a rigid object and perform coupled aerodynamic-rigid-object interaction simulations to investigate issues associated with VAWT self-starting. We also plan to include fluid-structure coupling in the modeling. The FSI issues in VAWTs are different than in HAWTs due to the differences in the topology of the structures employed. The flexibility in VAWTs does not come from the blades but rather the tower itself, and its connection to the rotor and ground. Finally, we would like to simulate small arrays of VAWTs to better understand wake effects and optimal positioning of turbines.

Acknowledgment

This work was supported through the National Science Foundation CAREER Award No. 1055091. The computational resources of the Texas Advanced Computing Center (TACC) were employed for the simulations reported in this work. This support is gratefully acknowledged.

References

[1] Hau, E., 2006, *Wind Turbines: Fundamentals, Technologies, Application, Economics*, 2nd ed., Springer, Berlin.
[2] Jonkman, J., Butterfield, S., Musial, W., and Scott, G., 2009, "Definition of a 5-MW Reference Wind Turbine for Offshore System Development," National Renewable Energy Laboratory, Golden, CO, Technical Report NREL/TP-500-38060.
[3] Klimas, P. C., 1982, "Darrieus Rotor Aerodynamics," ASME J. Solar Energ. Eng., **104**, pp. 102–105.
[4] Dabiri, J. O., 2011, "Potential Order-of-Magnitude Enhancement of Wind Farm Power Density Via Counter-Rotating Vertical-Axis Wind Turbine Arrays," J. Renew. Sustain. Energ., **3**, p. 043104.
[5] Takizawa, K., Bazilevs, Y., and Tezduyar, T. E., 2012, "Space–Time and ALE-VMS Techniques for Patient-Specific Cardiovascular Fluid–Structure Interaction Modeling," Arch. Comput. Meth. Eng., **19**, pp. 171–225.
[6] Bazilevs, Y., Hsu, M.-C., Takizawa, K., and Tezduyar, T. E., 2012, "ALE-VMS and ST-VMS Methods for Computer Modeling of Wind-Turbine Rotor Aerodynamics and Fluid–Structure Interaction," Math. Models Methods Appl. Sci., **22**(Supp. 02), p. 1230002.
[7] Bazilevs, Y., Hsu, M.-C., Akkerman, I., Wright, S., Takizawa, K., Henicke, B., Spielman, T., and Tezduyar, T. E., 2011, "3D Simulation of Wind Turbine Rotors at Full Scale. Part I: Geometry Modeling and Aerodynamics," Int. J. Num. Meth. Fluid., **65**, pp. 207–235.
[8] Hsu, M.-C., Akkerman, I., and Bazilevs, Y., 2011, "High-Performance Computing of Wind Turbine Aerodynamics Using Isogeometric Analysis," Comput. Fluid., **49**, pp. 93–100.
[9] Hsu, M.-C., Akkerman, I., and Bazilevs, Y., 2013, "Finite Element Simulation of Wind Turbine Aerodynamics: Validation Study Using NREL Phase VI Experiment," Wind Energy, (published online).
[10] Hsu, M.-C., Akkerman, I., and Bazilevs, Y., 2012, "Wind Turbine Aerodynamics Using ALE–VMS: Validation and the Role of Weakly Enforced Boundary Conditions," Comput. Mech., **50**, pp. 499–511.
[11] Bazilevs, Y., Hsu, M.-C., Kiendl, J., Wüchner, R., and Bletzinger, K.-U., 2011, "3D Simulation of Wind Turbine Rotors at Full Scale. Part II: Fluid–Structure Interaction Modeling With Composite Blades," Int. J. Num. Meth., **65**, pp. 236–253.
[12] Bazilevs, Y., Hsu, M.-C., and Scott, M. A., 2012, "Isogeometric Fluid–Structure Interaction Analysis With Emphasis on Non-Matching Discretizations, and With Application to Wind Turbines," Comput. Meth. Appl. Mech. Eng., **249–252**, pp. 28–41.
[13] Hsu, M.-C., and Bazilevs, Y., 2012, "Fluid–Structure Interaction Modeling of Wind Turbines: Simulating the Full Machine," Comput. Mech., **50**, pp. 821–833.
[14] Korobenko, A., Hsu, M., Akkerman, I., Tippmann, J., and Bazilevs, Y., 2013, "Structural Mechanics Modeling and FSI Simulation of Wind Turbines," Math. Models Methods Appl. Sci., **23**, pp. 249–272.
[15] Bazilevs, Y., and Hughes, T. J. R., 2008, "NURBS-Based Isogeometric Analysis for the Computation of Flows About Rotating Components," Comput. Mech., **43**, pp. 143–150.
[16] Bazilevs, Y., and Hughes, T. J. R., 2007, "Weak Imposition of Dirichlet Boundary Conditions in Fluid Mechanics," Comput. Fluid., **36**, pp. 12–26.
[17] Bazilevs, Y., Michler, C., Calo, V. M., and Hughes, T. J. R., 2007, "Weak Dirichlet Boundary Conditions for Wall-Bounded Turbulent Flows," Comput. Meth. Appl. Mech. Eng., **196**, pp. 4853–4862.
[18] Bazilevs, Y., Michler, C., Calo, V. M., and Hughes, T. J. R., 2010, "Isogeometric Variational Multiscale Modeling of Wall-Bounded Turbulent Flows With Weakly Enforced Boundary Conditions on Unstretched Meshes," Comput. Meth. Appl. Mech. Eng., **199**, pp. 780–790.
[19] Stein, P., Hsu, M.-C., Bazilevs, Y., and Beucke, K., 2012, "Operator- and Template-Based Modeling of Solid Geometry for Isogeometric Analysis With

Application to Vertical Axis Wind Turbine Simulation," Comput. Meth. Appl. Mech. Eng., **213–216**, pp. 71–83.
[20] Scheurich, F., Fletcher, T., and Brown, R., 2011, "Simulating the Aerodynamic Performance and Wake Dynamics of a Vertical-Axis Wind Turbine," Wind Energy, **14**, pp. 159–177.
[21] Scheurich, F., and Brown, R., 2013, "Modelling the Aerodynamics of Vertical-Axis Wind Turbines in Unsteady Wind Conditions," Wind Energy, **16**, pp. 91–107.
[22] McLaren, K., Tullis, S., and Ziada, S., 2012, "Computational Fluid Dynamics Simulation of the Aerodynamics of a High Solidity, Small-Scale Vertical Axis Wind Turbine," Wind Energy, **15**, pp. 349–361.
[23] Bravo, R., Tullis, S., and Ziada, S., 2007, "Performance Testing of a Small Vertical-Axis Wind Turbine," Proceedings of the 21st Canadian Congress of Applied Mechanics (CANCAM07), Toronto, Canada, June 3–7, pp. 470–471.
[24] Hughes, T. J. R., Liu, W. K., and Zimmermann, T. K., 1981, "Lagrangian–Eulerian Finite Element Formulation for Incompressible Viscous Flows," Comput. Meth. Appl. Mech. Eng., **29**, pp. 329–349.
[25] Bazilevs, Y., Takizawa, K., and Tezduyar, T., 2013, *Computational Fluid–Structure Interaction: Methods and Applications*, Wiley, Chichester, UK.
[26] Chung, J., and Hulbert, G. M., 1993, "A Time Integration Algorithm for Structural Dynamics With Improved Numerical Dissipation: The Generalized-α Method," ASME J. Appl. Mech., **60**, pp. 371–375.
[27] Jansen, K. E., Whiting, C. H., and Hulbert, G. M., 2000, "A Generalized-α Method for Integrating the Filtered Navier–Stokes Equations With a Stabilized Finite Element Method," Comput. Meth. Appl. Mech. Eng., **190**, pp. 305–319.
[28] Bazilevs, Y., Calo, V. M., Hughes, T. J. R., and Zhang, Y., 2008, "Isogeometric Fluid–Structure Interaction: Theory, Algorithms, and Computations," Comput. Mech., **43**, pp. 3–37.
[29] Tezduyar, T. E., 1992, "Stabilized Finite Element Formulations for Incompressible Flow Computations," Adv. Appl. Mech., **28**, pp. 1–44.
[30] Tezduyar, T. E., Behr, M., and Liou, J., 1992, "A New Strategy for Finite Element Computations Involving Moving Boundaries and Interfaces—The Deforming-Spatial-Domain/Space–Time Procedure: I. The Concept and the Preliminary Numerical Tests," Comput. Meth. Appl. Mech. Eng., **94**(3), pp. 339–351.
[31] Tezduyar, T. E., Behr, M., Mittal, S., and Liou, J., 1992, "A New Strategy for Finite Element Computations Involving Moving Boundaries and Interfaces—The Deforming-Spatial-Domain/Space–Time Procedure: II. Computation of Free-Surface Flows, Two-Liquid Flows, and Flows With Drifting Cylinders," Comput. Meth. Appl. Mech. Eng., **94**(3), pp. 353–371.
[32] Tezduyar, T. E., 2003, "Computation of Moving Boundaries and Interfaces and Stabilization Parameters," Int. J. Num. Meth. Fluid., **43**, pp. 555–575.
[33] Tezduyar, T. E., and Sathe, S., 2007, "Modeling of Fluid–Structure Interactions With the Space–Time Finite Elements: Solution Techniques," Int. J. Num. Meth. Fluid., **54**, pp. 855–900.
[34] Takizawa, K., and Tezduyar, T. E., 2011, "Multiscale Space–Time Fluid–Structure Interaction Techniques," Comput. Mech., **48**, pp. 247–267.
[35] Takizawa, K., Henicke, B. Tezduyar, T. E., Hsu, M.-C., and Bazilevs, Y., 2011, "Stabilized Space–Time Computation of Wind-Turbine Rotor Aerodynamics," Comput. Mech., **48**, pp. 333–344.
[36] Takizawa, K., Henicke, B., Montes, D., Tezduyar, T. E., Hsu, M.-C., and Bazilevs, Y., 2011, "Numerical-Performance Studies for the Stabilized Space–Time Computation of Wind-Turbine Rotor Aerodynamics," Comput. Mech., **48**, pp. 647–657.
[37] Takizawa, K., and Tezduyar, T. E., 2012, "Space–Time Fluid–Structure Interaction Methods," Math. Models Methods Appl. Sci., **22**(Supp. 02), p. 1230001.
[38] Tezduyar, T., Aliabadi, S., Behr, M., Johnson, A., Kalro, V., and Litke, M., 1996, "Flow Simulation and High Performance Computing," Comput. Mech., **18**, pp. 397–412.
[39] Behr, M., and Tezduyar, T., 1999, "The Shear-Slip Mesh Update Method," Comput. Meth. Appl. Mech. Eng., **174**, pp. 261–274.
[40] Behr, M., and Tezduyar, T., 2001, "Shear-Slip Mesh Update in 3D Computation of Complex Flow Problems With Rotating Mechanical Components," Comput. Meth. Appl. Mech. Eng., **190**, pp. 3189–3200.
[41] Tezduyar, T. E., 2001, "Finite Element Methods for Flow Problems With Moving Boundaries and Interfaces," Arch. Comput. Meth. Eng., **8**, pp. 83–130.
[42] Tezduyar, T. E., 2007, "Finite Elements in Fluids: Special Methods and Enhanced Solution Techniques," Comput. Fluid., **36**, pp. 207–223.
[43] Karypis, G., and Kumar, V., 1999, "A Fast and High Quality Multilevel Scheme for Partitioning Irregular Graphs," SIAM J. Sci. Comput., **20**, pp. 359–392.